Drug-target residence time : a case for the adenosine A1 and A2A receptors

Guo, D.

Chapter 5

Functional efficacy of adenosine A_{2A} receptor agonists is positively correlated to their receptor residence time

Guo D, Mulder-Krieger T, IJzerman AP, Heitman LH.
Adapted from: *Br J Pharmacol* 2012; 166(6): 1846-1859.

About this chapter

This chapter assesses the binding kinetics of $A_{2A}R$ agonists and explores a possible relationship with their functional efficacy. A kinetic radioligand binding assay (a so-called competition association assay) has been set up, validated and optimized at the $A_{2A}R$ to examine the binding kinetics of unlabeled ligands. Functional efficacies of $A_{2A}R$ agonists were determined in two different assays: a novel label-free impedance-based assay and a more traditional cAMP determination. A correlation was observed between the receptor residence time of $A_{2A}R$ agonists and their intrinsic efficacies in both functional assays. The affinity of $A_{2A}R$ agonists was not correlated to their functional efficacy. This study indicates that the molecular basis of different agonist efficacies at the $A_{2A}R$ lies within their different residence times at this receptor.

5.1 Introduction

Extracellular adenosine is a ubiquitous local hormone that has been reported to play an important physiological role in numerous tissues, for instance in the sleep/wake cycle and in inflammation. The nucleoside can bind and activate four subtypes of adenosine receptors.[1] These are the adenosine A_1, A_{2A}, A_{2B} and A_3 receptors, which belong to the superfamily of G protein-coupled receptors (GPCRs). The adenosine A_1 and A_3 receptors are mainly coupled to the enzyme adenylate cyclase in an inhibitory fashion via a G_i protein, whereas the A_{2A} and A_{2B} receptors stimulate this enzyme via a G_s protein.[2] In this study we focused on agonists for the human adenosine A_{2A} receptor ($hA_{2A}R$), which have clinical relevance in various pathological conditions such as respiratory disorders and inflammatory conditions.[3]

Traditionally, drug discovery campaigns of $A_{2A}R$ (and other GPCRs) agents usually include the identification of lead compounds in a dose-dependent assessment of activities (i.e., EC_{50} or K_i values) under equilibrium conditions. The binding kinetics of the drug-target interaction are usually not taken into account. However, awareness of the importance of binding kinetics has started to increase, since accumulating evidence suggests that the *in vivo* effectiveness of ligands may be attributed to the time ligands reside at their receptor.[4-7] The duration a drug stays in complex with the target is defined as 'drug-target residence time', which equals the reciprocal of the dissociation rate constant ($1 / k_{off}$).[8]

A recent study at the muscarinic M_3 receptor showed a tight correlation between receptor residence time and agonist efficacy.[9] This finding suggests that the molecular basis behind ligand efficacy may be inextricably linked to the ligand-receptor residence time. To verify this possible relationship, we determined the binding kinetics of ten $A_{2A}R$ agonists from different chemical classes (Figure 5.1) and extensively explored the putative relationship to their functional efficacies at the $hA_{2A}R$. The agonist binding kinetics were quantified using a competition association method,[10] which we adopted and further optimized into a fast, medium-throughput format. The $A_{2A}R$ agonist efficacies were measured, for the first time, in a novel label-free impedance-based assay and in a 'traditional' cAMP assay.

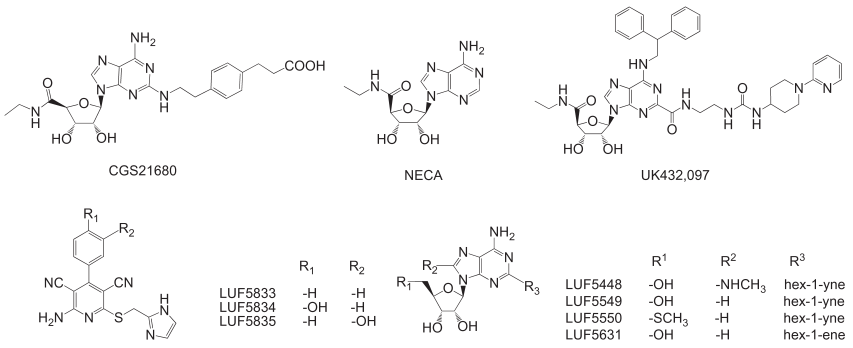

Figure 5.1 | Chemical structures of ten $A_{2A}R$ agonists used in this chapter.

5.2 Methods

Chemicals and reagents

[^{3}H]-ZM241385 (specific activity 28.4 Ci/mmol) was purchased from ARC Inc. (St. Louis, USA). Unlabeled ZM241385 was a gift from Dr. S. M. Poucher (Astra-Zeneca, Macclesfield, UK). CGS21680 was a gift from Dr. R. A. Lovell (Ciba-Geigy, Summit, NJ). NECA was purchased from Sigma-Aldrich (Steinheim, Germany), UK432,097 was purchased from Axon (Groningen, Netherlands). LUF5448 and LUF5631 were synthesized in our laboratory as described previously by van Tilburg *et al.*[11]; LUF5549 and LUF5550 were described by van Tilburg *et al.*[12]; LUF5833, LUF5834 and LUF5835 were described by Beukers *et al.*[13]. Guanosine triphosphate (GTP) was purchased from Acros Organics (Geel, Belgium). Adenosine deaminase (ADA) was purchased from Boehringer Mannheim (Mannheim, Germany). Bicinchoninic acid (BCA) and BCA protein assay reagent were obtained from Pierce Chemical Company (Rockford, IL, U.S.A.). Human embryonic kidney 293 cells stably expressing the $hA_{2A}R$ (HEK293$hA_{2A}R$) were kindly provided by Dr. J Wang (Biogen/IDEC, Cambridge, MA). All other chemicals were of analytical grade and obtained from standard commercial sources.

Cell culture

HEK293hA_{2A}R cells were grown in culture medium consisting of Dulbecco's Modified Eagle's Medium (DMEM) supplemented with 10% newborn calf serum (NCS), 50 μg/mL streptomycin, 50 IU/mL penicillin, and 500 μg/mL G418 at 37 ˚C and 7% CO_2. Cells were subcultured twice a week at a ratio of 1:8 on 10 cm ø plates.

Cell membrane preparation

HEK293hA_{2A}R cells were grown to 80%-90% confluency and detached from plates by scraping them into 5 mL PBS. Detached cells were collected and centrifuged at 700×g (3000 r.p.m.) for 5 min. Pellets derived from 30 plates (15 cm ø) were pooled and resuspended in 20 mL of ice-cold 25 mM Tris-HCl buffer, pH 7.4. An UltraThurrax was used to homogenize the cell suspension. Membranes and the cytosolic fraction were separated by centrifugation at 100,000×g (31,000 r.p.m.) in a Beckman Optima LE-80K ultracentrifuge at 4 ˚C for 20 min. The pellet was resuspended in 10 mL of Tris buffer and the homogenization and centrifugation step was repeated. Tris buffer (10 mL) was used to resuspend the pellet and ADA was added (0.8 IU/mL) to break down endogenous adenosine. Membranes were stored in 250 μL aliquots at -80 ˚C. Membrane protein concentrations were measured using the BCA (bicinchoninic acid) method.[14]

Radioligand saturation and displacement assays

Membrane aliquots containing 20 μg of protein were incubated in a total volume of 100 μl of assay buffer (25 mM Tris-HCl, pH 7.4, supplemented with 5 mM $MgCl_2$ and 0.1% (w/v) 3-[(3-cholamidopropyl) dimethylammonio]-1-propanesulfonate (CHAPS) at 5 ˚C for 2 hours to ensure the equilibrium was reached at all concentrations of radioligand. For saturation experiments,

a range of concentrations (~0.2-10 nM) of [^{3}H]-ZM241385 was used. Nonspecific binding was determined at three concentrations of radioligand in the presence of 100 μM CGS21680. Radioligand displacement experiments were performed using eleven concentrations of competing ligand in the presence of 5.5 nM [^{3}H]-ZM241385. In such experiments ZM241385 and NECA were tested in the absence or presence of 100 μM GTP. Nonspecific binding was determined in the presence of 100 μM CGS21680 and represented less than 10% of the total binding. [^{3}H]-ZM241385 did not bind specifically to membranes prepared from parental HEK293 cells. Incubations were terminated by rapid vacuum filtration to separate the bound and free radioligand through 96-well GF/B filter plates using a Perkin Elmer Filtermate-harvester (Perkin Elmer, Groningen, Netherlands) after the indicated incubation time. Filters were subsequently washed three times with ice-cold wash buffer (25 mM Tris HCl, pH 7.4, supplemented with 5 mM $MgCl_2$). The filter-bound radioactivity was determined by scintillation spectrometry using the P-E 1450 Microbeta Wallac Trilux scintillation counter (Perkin Elmer, Groningen, Netherlands).

Radioligand association and dissociation assays

Association experiments were performed by incubating membrane aliquots containing 20 μg of protein in a total volume of 100 μl of assay buffer (25 mM Tris-HCl, pH 7.4, supplemented with 5 mM $MgCl_2$ and 0.1% CHAPS) at 25 ˚C or 5 ˚C with 5.5 nM [^{3}H]-ZM241385. The amount of radioligand bound to the receptor was measured at different time intervals during incubation for 30 min at 25 ˚C or 2 hours at 5 ˚C. Dissociation experiments were performed by pre-incubating membrane aliquots containing 20 μg of protein in a total volume of 100 μl of assay buffer (25 mM Tris-HCl, pH 7.4, supplemented with 5 mM $MgCl_2$ and 0.1% CHAPS) either at 25 ˚C for 30 minutes or at 5 ˚C for 2 hours with 5.5 nM [^{3}H]-ZM241385. After the pre-incubation, the dissociation was initiated by addition of 1 μM of unlabeled ZM241385 in 5 μL. The amount of radioligand still bound to the receptor was measured at various time intervals for a total duration of 30 min at 25 ˚C or 4 hours at 5 ˚C to ensure that [^{3}H]-ZM241385 was fully dissociated from the $hA_{2A}R$. Incubations were terminated and samples were obtained as described under *Radioligand saturation and displacement assays.*

Radioligand competition association assay

The binding kinetics of unlabeled ligands were determined at 5 ˚C using the competition association assay as developed by Motulsky and Mahan.[10] In the standard assay, three different concentrations of unlabeled ZM241385 or NECA were tested, namely at 1-, 3- and 10-fold its K_i value. For NECA its kinetics were also determined in the presence of 100 μM GTP. We also assessed binding kinetics in a simplified one-concentration competition association assay, at only 10-fold of the respective K_i value of the unlabeled ligands. The experiment was initiated by adding membrane aliquots containing 20 μg of protein at different time points. Incubations were terminated and samples were obtained as described under *Radioligand saturation and displacement assays*.

Label-free whole cell analysis (xCELLigence RTCA system)

Whole cell assays were performed on the xCELLigence RTCA system.[15,16] Briefly, a monolayer of cells adheres to an arrayed microelectrode embedded at the bottom of each well of an E-plate 96 (Roche Applied Science, Germany), which is compatible with the xCELLigence RTCA system. Upon activation of GPCR-mediated signaling, cell morphology changes and thereby affects the local ionic environment at the cell-electrode interface. This leads to an increased electronic readout of cell-sensor impedance (Z), which is displayed in real-time as the Cell Index (CI). Specifically, the CI value at each time point is defined as $(Z_i\text{-}Z_0)$ Ω /15 Ω, where Z_i is the impedance at each individual time point, and Z_0 is the impedance derived from electrode/solution interface in the absence of cells prior to the start of the experiment. Thus, a loss of adhesion would generate a lower CI; an increase in cell adhesion, which is typical seen with GPCR-mediated activation, results in an overall increase in the CI.[17-19]

HEK293hA_{2A}R cells were cultured as a monolayer on 10 cm ø culture plates to 80%-90% confluency and subsequently harvested and centrifuged two times at 1000 r.p.m for 5 min. Initially, 45 μL of culture media was added to wells in E-Plates 96 to obtain background readings (Z_0) followed by the addition of 50 μL of cell suspension containing 20,000 cells / well.

The E-plate containing the cells was left at room temperature for 15 min before being placed on the recording device station in the incubator at 37 ˚C in 5% CO_2. Afterwards, cell attachment, spreading and proliferation were continuously monitored every 30 minutes. The cells were cultured until the end of log phase (~18-20 h) to obtain an optimal assay window. Prior to agonist application the interval between two measurements was adjusted to 1 min. Subsequently 5 µL compound solution (final concentration of 0.5 % DMSO) or vehicle control was added to each well, after which the CI was recorded for 30 minutes. For data analysis the individual CI traces were normalized by subtracting the baseline (vehicle control) to correct for any agonist-independent signals.

cAMP assay

HEK293hA_{2A}R cells were cultured as a monolayer on 10 cm ø culture plates to 80%-90% confluency. Cells were harvested and centrifuged two times at 1000 r.p.m for 5 min. The amount of cAMP produced was determined with the LANCE cAMP 384 kit (Perkin-Elmer, Groningen, Netherlands). In short, 2500 cells/well were pre-incubated for 45 min at 37 ˚C and subsequently at room temperature for three hours with a range of agonist concentrations. cAMP generation was performed in the medium containing cilostamide (50 µM), rolipram (50 µM), and adenosine deaminase (0.8 IU/mL). The incubation was stopped by adding detection mix and antibody solution, according to the instructions of the manufacturer. The generated fluorescence intensity was quantified on the EnVision® Multilabel Reader (PerkinElmer, Groningen, Netherlands). cAMP production by agonists tested at 100-fold their K_i value on the parental HEK293 cell line represented less than 5% of maximal stimulation of cAMP production by 10 µM CGS21680 at the cells expressing the adenosine A_{2A} receptor.

Data analysis

All experimental data was analyzed by using GraphPad Prism 5.0 (GraphPad Software Inc., San Diego, CA). K_D and B_{max} values of [^{3}H]-ZM241385 at

$hA_{2A}R$ membranes were obtained by computational analysis of saturation curves. IC_{50} values obtained from competition displacement binding data were converted into K_i values using the Cheng-Prusoff equation.[20]

Association data was fitted using *one phase exponential association*. Values for k_{on} were obtained by converting k_{obs} values using Equation 3 describe in Chapter 3. k_{off} values were assessed from independent dissociation experiments. Dissociation data was fitted using *one phase exponential decay*. The association and dissociation rates were used to calculate the 'kinetic K_D' using Equation 8 described in Chapter 3.

Association and dissociation rates for unlabeled ligands were calculated by fitting the data in the competition association model using '*kinetics of competitive binding*' describe in Chapter 3 (Equation 7).[10]

EC_{50} and E_{max} values in label-free whole cell assay were obtained by analyzing the normalized CI traces using RTCA Software 1.2 (Roche, Germany) to obtain peak responses within 30 min after compound addition. These peak values were exported to Prism 5.0, which yielded dose-response curves and were analyzed by nonlinear regression.

The relative efficacies (τ) of agonists in label-free whole cell experiment and cAMP assay were also evaluated. Data were fitted to the operational model of Black and Leff,[21] which correlates a biological effect E with agonist concentration [A] as a function of three parameters: E_m, K_A, and τ:

$$E = \frac{E_m \cdot \tau \cdot [A]}{K_A + (\tau + 1)[A]}$$

where E_m, the operational maximum, represents the maximum possible effect in the tissue. K_A is the dissociation constant of agonist and τ is the relative efficacy. The E_m value was generated by fitting the dose-response curve for the full agonist (i.e., UK432,097). Its best-fit values were recorded to fit dose-response curves of partial agonists and other full agonists by global fitting in the operational model in Prism 5.0 to generate their relative efficacies. All values obtained are means of at least three independent experiments performed in duplicate.

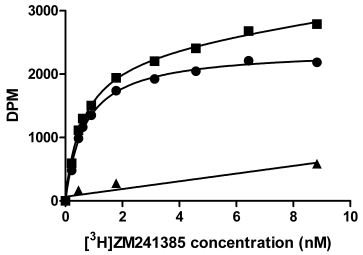

Figure 5.2 | Saturation experiment of [^{3}H]-ZM241385 (~0.2-10 nM, final concentration) binding to HEK293hA_{2A}R membranes at 5 °C, total binding (squares); non-specific binding (triangles); specific binding (spheres). Representative graph from one experiment performed in duplicate.

5.3 Results

Quantification of the K_D and B_{max} of [^{3}H]-ZM241385 in saturation experiments

Saturation binding experiments were performed with [^{3}H]-ZM241385 at 5 °C. The result of a representative saturation experiment is shown in Figure 5.2. [^{3}H]-ZM241385 bound to a single class of binding sites at HEK293hA_{2A}R membranes. The K_D value was determined as 0.60 ± 0.07 nM and B_{max} was 1.9 ± 0.04 pmol/mg protein. The K_D value for [^{3}H]-ZM241385 obtained with these experiments was used to derive K_i values from IC_{50} values for ten A_{2A}R agonists, as well as the unlabeled antagonist ZM241385 (see below).

Quantification of the affinity (K_i) of A_{2A}R ligands in displacement experiments

Displacement experiments with several A_{2A}R ligands were performed to determine their affinities to the hA_{2A}R. All compounds produced a concentration-dependent inhibition of specific [^{3}H]-ZM241385 binding

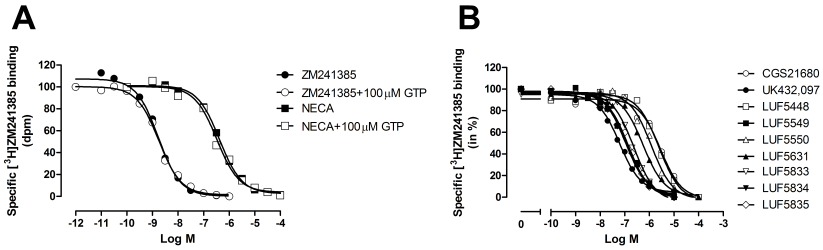

Figure 5.3 | Panel A: displacement of specific [^{3}H]-ZM241385 binding from the $hA_{2A}R$ by ZM241385 and NECA in the absence (closed symbols) or presence of 100 μM GTP (open symbols). Panel B: displacement of specific [^{3}H]-ZM241385 binding from the $hA_{2A}R$ by the other nine agonists. Representative graphs from one experiment performed in duplicate.

(Figure 5.3) and their affinities are detailed in Table 5.1 and Table 5.3. Amongst all tested ligands, ZM241385 showed the highest affinity for the $hA_{2A}R$ with a K_i value of 0.4 ± 0.03 nM (Table 5.1) in the absence of 100 μM GTP; its K_i value determined in the presence of 100 μM GTP was the same (0.4 ± 0.02 nM, Figure 5.3A). Similarly, there was no significant difference between the kinetic or K_i values of NECA tested in the absence or presence of 100 μM GTP (Tables 5.2 and 5.3, Figure 5.3A). Affinities of other $A_{2A}R$ agonists were determined and showed a range of K_i values in the lower to higher nanomolar range (Table 5.3). The agonist with the lowest affinity was CGS21680 (K_i = 376 ± 12 nM), while the agonist with the highest affinity was LUF5835 (K_i =15 ± 4 nM). In general, the affinities of the ribose-containing agonists (e.g., LUF5448) were lower than those of the non-ribose agonists (e.g., LUF5833), as shown in Table 5.3.

Quantification of the association [k_{on} (k_1)] and dissociation rates [k_{off} (k_2)] of [^{3}H]-ZM241385 at different temperatures

To optimize the experimental conditions of the kinetic binding assays, [^{3}H]-ZM241385 association and dissociation experiments were carried out at both 25 ˚C and 5 ˚C. At both temperatures, the association and dissociation curve of [^{3}H]-ZM241385 at the $hA_{2A}R$ were monophasic. At 25 ˚C (Figure

Table 5.1 | Comparison of the affinity, dissociation constants and kinetic rates of reference antagonist ZM241385 obtained in different radioligand binding assays.

Assay	K_D / K_i *(nM)*	k_{on} *(M^{-1}·min^{-1})*	k_{off} *(min^{-1})*
Saturation binding [a]	0.60 ± 0.07	*N.A*	*N.A*
Displacement [b]	0.40 ± 0.03	*N.A*	*N.A*
Association and dissociation [c]	0.70 ± 0.01	1.5 ± 0.06 × 10^7	0.011 ± 0.001
Standard competition association [d]	0.95 ± 0.2[f]	2.0 ± 0.2 × 10^7	0.019 ± 0.003
Simplified competition association [e]	0.89 ± 0.3[f]	2.8 ± 0.5 × 10^7	0.025 ± 0.006

Values are means ± s.e.m of three separate experiments each performed in duplicate. *N.A.*, not applicable. [a] [^{3}H]-ZM241385 (~0.2-10 nM) binding to HEK293hA_{2A} membranes at 5 ˚C. [b] Displacement of specific [^{3}H]-ZM241385 binding from the hA_{2A}R at 5 ˚C. [c] Association and dissociation of [^{3}H]-ZM241385 at the hA_{2A}R at 5 ˚C. [d] The binding kinetics of unlabeled ZM241385 were determined by adding a concentration equivalent to 1-, 3- and 10-fold the K_i value of unlabeled ZM241385 at 5 ˚C. [e] The binding kinetics of unlabeled ZM241385 were determined by adding a concentration equivalent to only 10-fold the K_i value of unlabeled ZM241385 at 5 ˚C. [f] 'kinetic K_D' = k_{off} / k_{on}.

5.4A), [^{3}H]-ZM241385 had a very fast association (k_{on} = 2.4 ± 0.05 × 10^8 M^{-1}·min^{-1}) and dissociation rate (k_{off} = 0.48 ± 0.03 min^{-1}). Decreasing the experimental temperature to 5 ˚C resulted in slower binding kinetics of [^{3}H]-ZM241385 with an association rate of 1.5 ± 0.06 × 10^7 M^{-1}·min^{-1} and a dissociation rate of 0.011 ± 0.001 min^{-1} (Figure 5.4B, Table 5.1). We also conducted experiments at 15 ˚C; the kinetic rates determined were also fast (data not shown). Based on these initial tests, we chose 5 ˚C as the standard experimental condition for this study, since it enabled better accuracy and reproducibility of kinetic data.

Validation and optimization of the competition association assay at the hA_{2A}R

With the pre-determined k_{on} (k_1) and k_{off} (k_2) values of [^{3}H]-ZM241385 from association and dissociation experiments, k_{on} (k_3) and k_{off} (k_4) values of unlabeled ligands could be determined by fitting the kinetic parameters into the model of '*kinetics of competitive binding*' described in *methods*. Firstly,

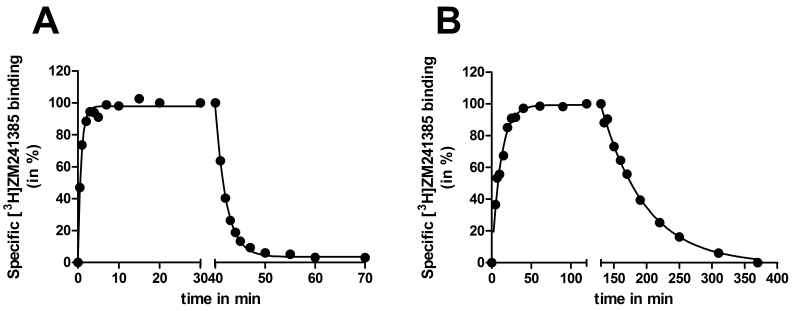

Figure 5.4 | Panel A: the association and dissociation of [^{3}H]-ZM241385 at the $hA_{2A}R$ at 25 ˚C; Panel B: the association and dissociation of [^{3}H]-ZM241385 at the $hA_{2A}R$ at 5 ˚C. Representative graphs from one experiment performed in duplicate.

we validated the competition association assay at the $hA_{2A}R$ using unlabeled ZM241385. Its k_{on} (k_3) and k_{off} (k_4) values determined in this assay were $2.0 \pm 0.2 \times 10^7$ $M^{-1}\cdot min^{-1}$ and 0.019 ± 0.003 min^{-1} respectively (Figure 5.5, Table 5.1), which corresponded rather well to the kinetic rates determined in 'traditional' association and dissociation experiments described in the previous paragraph ($k_{on} = 1.5 \pm 0.06 \times 10^7$ $M^{-1}\cdot min^{-1}$, $k_{off} = 0.011 \pm 0.001$ min^{-1}). Moreover, the 'kinetic K_D' (0.95 ± 0.2 nM) derived from the competition association assay for unlabeled ZM241385 was similar to the affinity constant ($K_i = 0.40 \pm 0.03$ nM) obtained from displacement experiments and the dissociation constant (K_D) derived from saturation experiments (0.60 ± 0.07 nM, Table 5.1). Taken together, this proved that the competition association assay can be applied to determine the binding kinetics of unlabeled ligands at the $hA_{2A}R$.

Secondly, we modified the assay and improved its throughput by reducing the three-concentration dependent method to a one-concentration based method. Instead of testing at concentrations equivalent to 1-, 3- and 10-fold the K_i value of unlabeled ZM241385, we only used 10-fold K_i. The latter yielded an assay window distinguishable from both the baseline and the control curve (Figure 5.5). Specifically, the data analyzed at 10-fold K_i alone of unlabeled ZM241385 showed a comparable result ($k_{on} = 2.8 \pm 0.5 \times 10^7$ $M^{-1}\cdot min^{-1}$, $k_{off} = 0.025 \pm 0.006$ min^{-1}) to that generated in a standard (three concentration) competition association experiment (Table 5.1).

Next to that, we also determined the effect of GTP (100 μM) on the

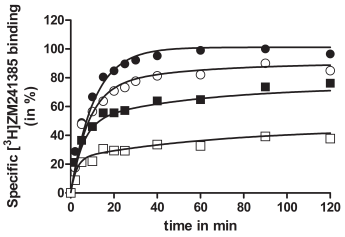

Figure 5.5 | Competition association experiment with [^{3}H]-ZM241385 in the absence of ligand (solid spheres) or in the presence of one-fold K_i value (empty spheres), three-fold K_i value (solid squares) or ten-fold K_i value (empty squares) of unlabeled ZM241385. Representative graphs from one experiment performed in duplicate (see Table 5.1 for kinetic values).

binding kinetics of an unlabeled agonist, NECA. Its k_{on} and k_{off} values determined in the standard three-concentration competition association assay in the absence of GTP were 8.1 ± 1.0 × 10^5 M^{-1}·min^{-1} and 0.038 ± 0.007 min^{-1} (Table 5.2, Figure 5.6A), which were similar to these values determined in the presence GTP (k_{on} = 9.8 ± 1.0 × 10^5 M^{-1}·min^{-1}, k_{off} = 0.036 ± 0.006 min^{-1}, Table 5.2, Figure 5.6B). Furthermore, k_{on} and k_{off} values of unlabeled NECA assessed by using a concentration of 10-fold its K_i only, either in the absence or presence of 100 μM GTP, showed comparable results to that determined by the standard assay mentioned above (Table 5.2). It is also noteworthy that the calculated kinetic K_D values from the one-concentration approach in the absence (K_D = 58 nM) or presence (K_D = 52 nM) of GTP are almost identical to the affinity determined in the displacement experiments (K_i = 64 ± 1 nM). Thus, the simplified one-concentration competition association assay in the absence of 100 μM GTP was used to determine the binding kinetics of other unlabeled agonists in the rest of this study.

Quantification of the binding kinetics of unlabeled ligands using the simplified competition association assay

By using the simplified competition association assay, the on- and off-rates of ten $A_{2A}R$ agonists were determined. Notably, a good correlation (Figure 5.7B, r^2 = 0.99, p < 0.0001) was observed between the affinities (K_i) determined

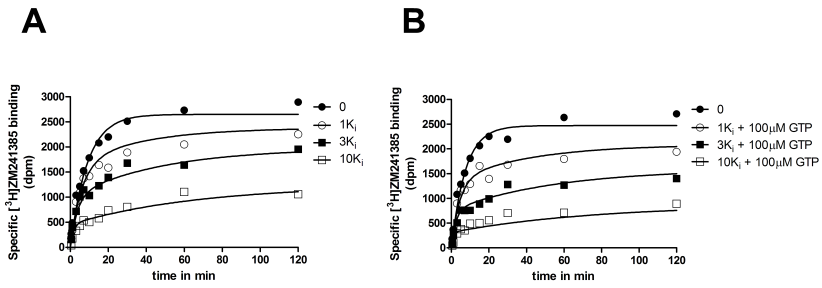

Figure 5.6 | [^{3}H]-ZM241385 competition association experiments in the absence (Panel A) or presence (Panel B) of 100 μM GTP with NECA concentrations of one, three or ten-fold its K_i value. Data were fitted to the equations described in *Methods* to calculate NECA's k_{on} and k_{off} values in the absence or presence of GTP. Representative graphs from one experiment performed in duplicate (see Table 5.2 for kinetic values).

Table 5.2 | The binding kinetics of reference agonist NECA in the absence or presence of 100 μM GTP.

Assay	***Control***		***+ 100 μM GTP***	
	k_{on} ($M^{-1}{\cdot}min^{-1}$)	k_{off} (min^{-1})	k_{on} ($M^{-1}{\cdot}min^{-1}$)	k_{off} (min^{-1})
Standard competition association [a]	8.1 ± 1.0 × 10^5	0.038 ± 0.007	9.8 ± 1.0 × 10^5	0.036 ± 0.006
Simplified competition association [b]	5.0 ± 0.6×10^5	0.029 ± 0.005	9.1 ± 2.0 × 10^5	0.047 ± 0.01

Values are means ± s.e.m of three separate experiments each performed in duplicate. [a] The binding kinetics of unlabeled NECA in the absence or presence of 100 μM GTP were determined by adding a concentration equivalent to 1-, 3- and 10-fold the K_i value of unlabeled NECA in the absence or presence of 100 μM GTP at 5 ˚C. [b] The binding kinetics of unlabeled NECA in the absence or presence of 100 μM GTP were determined by adding a concentration equivalent to only 10-fold the K_i value of unlabeled NECA in the absence or presence of 100 μM GTP at 5 ˚C.

in equilibrium binding studies and K_D values derived from the competition association assays (Table 5.3). This further proved that the simplified model is able to accurately quantify the association and dissociation rates of unlabeled ligands. Two distinct patterns of [^{3}H]-ZM241385 binding were found in the presence of the agonists, which are depicted in Figure 5.7A: 1) the specific binding of [^{3}H]-ZM241385 approached its equilibrium slowly and more gradually if [^{3}H]-ZM241385 dissociated slower than the competitor

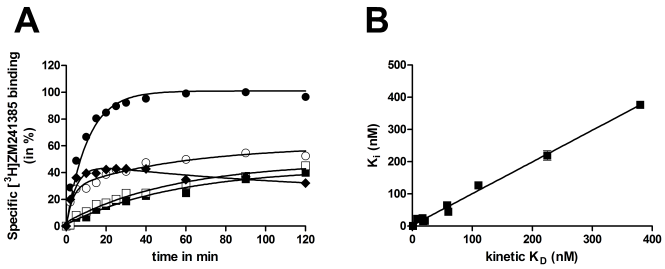

Figure 5.7 | Quantification of the binding kinetics of unlabeled ligands using the simplified competition association assay. Panel A, [^{3}H]-ZM241385 competition association binding in the absence of ligand (solid spheres) or in the presence of unlabeled CGS21680 (empty spheres), LUF5834 (solid squares), LUF5550 (empty squares) or UK432,097 (solid diamonds). Data were fitted to the equations described in *Methods* to calculate the k_{on} and k_{off} values of unlabeled ligands. Representative graphs from one experiment performed in duplicate (see Table 5.3 for kinetic values); Panel B, correlation between affinities (K_i) and 'kinetic K_D' values of all the tested compounds. K_i values were taken from the displacement experiments at equilibrium and K_D values were derived from the competition association experiments.

Table 5.3 | Binding parameters for agonists at HEK293hA_{2A}R derived from the simplified competition association assay and equilibrium radioligand displacement experiments.

Cmpd	*k_{on} (M^{-1}·min^{-1}) [a]*	*k_{off} (min^{-1}) [a]*	*RT (min) [b]*	*Kinetic K_D (nM) [c]*	*K_i (nM) [d]*
CGS21680	5.0 ± 1.0 × 10^4	0.019 ± 0.004	53 ± 6	380 ± 66	376 ± 12
NECA	5.0 ± 0.6 × 10^5	0.029 ± 0.005	35 ± 4	58 ± 7	64 ± 1
UK432,097	5.0 ± 0.8 × 10^5	0.004 ± 0.003	250 ± 115	8.0 ± 3.7	22 ± 5
LUF5448	2.8 ± 0.1 × 10^5	0.063 ± 0.020	16 ± 3	225 ± 39	219 ± 15
LUF5549	2.4 ± 0.5 × 10^6	0.041 ± 0.010	24 ± 3	17 ± 2	24 ± 7
LUF5550	8.0 ± 2.0 × 10^5	0.087 ± 0.020	12 ± 1	110 ± 19	126 ± 10
LUF5631	8.0 ± 2.0 × 10^5	0.048 ± 0.020	21 ± 5	60 ± 17	44 ± 9
LUF5833	8.5 ± 3.0 × 10^6	0.16 ± 0.08	6.3 ± 1.8	19 ± 7	17 ± 4
LUF5834	1.1 ± 0.4 × 10^7	0.23 ± 0.10	4.2 ± 1.0	21 ± 7	16 ± 5
LUF5835	1.6 ± 0.8 × 10^7	0.29 ± 0.10	3.4 ± 0.6	18 ± 6	15 ± 4

Data are shown as mean ± s.e.m of three separate experiments each performed in duplicate. [a] k_{on} and k_{off} of unlabeled A_{2A}R agonists were determined in one-concentration competition association assay. [b] RT (Residence Time) = 1 / k_{off}. [c] Kinetic K_D = k_{off} / k_{on}. [d] Displacement of specific [^{3}H]-ZM241385 binding from the hA_{2A}R at 5 °C.

($k_2 < k_4$, e.g., LUF5834); 2) the specific binding [^{3}H]-ZM241385 became biphasic with a typical 'overshoot' followed by a continuous decline towards equilibrium if [^{3}H]-ZM241385 dissociated faster than the competitor ($k_2 > k_4$, e.g., UK432,097). In accordance with these observations, UK432,097 had a much slower off-rate (k_{off} = 0.004 ± 0.003 min^{-1}) than [^{3}H]-ZM241385 (k_{off} = 0.011 ± 0.001 min^{-1}). LUF5834 (k_{off} = 0.23 ± 0.10 min^{-1}) or LUF5550 (k_{off} = 0.087 ± 0.020 min^{-1}) dissociated much faster from the receptor than [^{3}H]-ZM241385. Furthermore, it follows from Table 5.3 that the values for binding kinetics of ribose-containing agonists were significantly different from those of non-ribose agonists. For instance, LUF5631 was 10-fold slower in association and 3.3-fold slower in dissociation compared to LUF5833.

Quantification of functional efficacies of $A_{2A}R$ agonists in a label-free whole cell assay

Changes in cell morphology by the addition of CGS21680 and other $A_{2A}R$ agonists to HEK293h$A_{2A}R$ cells were assessed in real-time with the impedance-based assay system. Typically, upon agonist addition to HEK293h$A_{2A}R$ cells the impedance (displayed as cell index, CI) resulted in an immediate dose-dependent increase to a peak level. After that, the CI trace decreased and gradually reached a plateau without returning to the baseline when monitored over a period of 30 min. A representative measurement of CGS21680-induced impedance changes is plotted in Figure 5.8A. Concentration-effect curves were obtained from peak analysis of corresponding agonist-induced CI changes (Figure 5.8B). Agonist potencies, intrinsic efficacies and their relative efficacies (τ) analyzed in the operational model are detailed in Table 5.4. Specifically, amongst all tested agonists, UK432,097 had the highest efficacy, with a value of 114 ± 4% compared to the reference agonist CGS21680 (set at 100%). Efficacies of other ribose-containing agonists LUF5448, LUF5549, LUF5550 and LUF5631 were 83 ± 5%, 92 ± 4%, 63 ± 6% and 91 ± 8%, while the efficacies of the non-ribose agonists LUF5833, LUF5835 and LUF5834 were 54 ± 9%, 47 ± 6% and 54 ± 8%, respectively. In Figure 5.9A and 5.9B, correlations are shown between the agonist efficacy and either their affinities or receptor residence times, respectively. It follows from Figure 5.9A that there was very little correlation between the affinity of the agonists and their efficacy, if at all (r^2 = 0.13, p = 0.32). Interestingly, when the efficacy

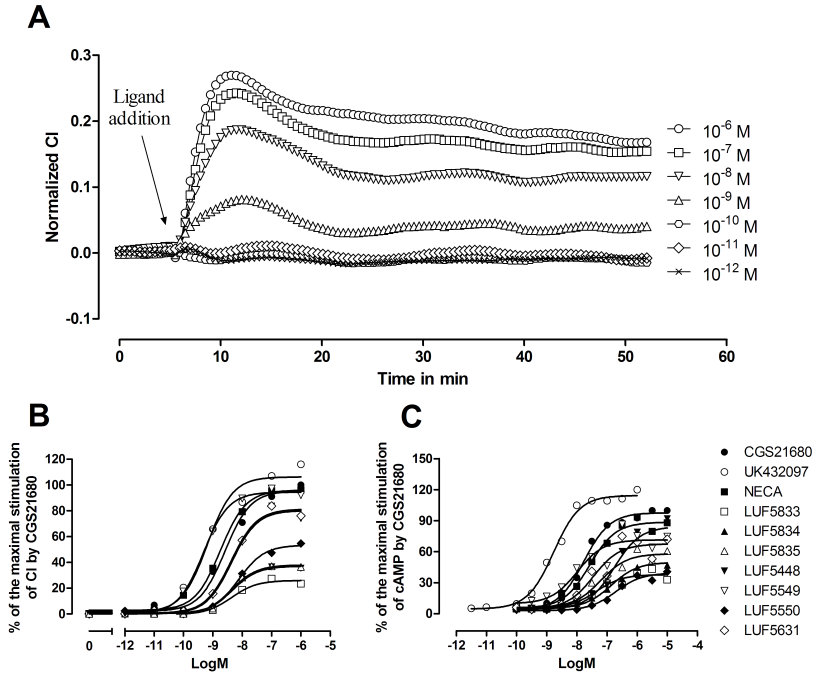

Figure 5.8 | Quantification of functional efficacies of $A_{2A}R$ agonists in a label-free whole cell assay. Panel A, representative graph of normalized cell-electrode impedance (expressed as CI) after the addition of different concentrations of CGS21680 in a label-free impedance-based assay: agonist stimulation of HEK293 $hA_{2A}R$ cells results in an increased CI. The change in CI was normalized over time against the vehicle control. Panel B, concentration-response curves for difference $A_{2A}R$ agonists at HEK293$hA_{2A}R$ derived from peak-analysis of CI changes in the xCELLigence RTCA system. The cellular response was normalized and shown as % of the maximal CI by 1 μM CGS21680; Panel C, concentration-response curves of cAMP stimulation by ten $A_{2A}R$ agonists in a cAMP assay. Data were normalized and shown as % of the maximal cAMP production by 10 μM CGS21680 in HEK293 $hA_{2A}R$ cells (= 100%). Representative graphs from one experiment performed in duplicate.

Table 5.4 | Agonist potency and efficacy derived from both cAMP and label-free whole cell assays.

Agonist	*Label-free whole cell assay* [a]			*cAMP assay*		
	EC_{50}, nM	E_{max}, %	τ [b]	EC_{50}, nM	E_{max}, %	τ [b]
CGS21680	3.8 ± 0.4	100 ± 1	13 ± 5	19 ± 0.6	100 ± 2	4 ± 0.4
NECA	2.5 ± 0.1	90 ± 4	4 ± 0.8	27 ± 0.9	88 ± 3	3 ± 0.3
UK432,097	0.47 ± 0.01	114 ± 4	51 ± 5	1.7 ± 0.1	115 ± 2	14 ± 5
LUF5448	2.4 ± 1	83 ± 5	2 ± 0.4	172 ± 15	84 ± 3	2 ± 0.4
LUF5549	1.0 ± 0.4	92 ± 4	6 ± 0.8	10 ± 3	71 ± 6	1 ± 0.2
LUF5550	5.8 ± 1	63 ± 6	0.7 ± 0.07	195 ± 12	39 ± 1	0.5 ± 0.04
LUF5631	4.3 ± 1	91 ± 8	2 ± 0.3	36 ± 23	67 ± 5	1 ± 0.2
LUF5833	3.9 ± 0.6	54 ± 9	1 ± 0.3	44 ± 2	38 ± 2	0.5 ± 0.04
LUF5834	3.6 ± 0.7	47 ± 6	0.8 ± 0.2	21 ± 1	50 ± 1	0.7 ± 0.06
LUF5835	5.7 ± 2	54 ± 8	0.8 ± 0.08	17 ± 1	58 ± 2	0.9 ± 0.09

Data are shown as mean ± s.e.m of three separate experiments each performed in duplicate. [a] agonist potency (EC_{50}) and efficacy (E_{max}) were calculated from concentration-response curves derived from peak-analysis of CI changes. [b] The relative efficacy (τ) was analyzed by the operational model of Black and Leff using global fitting.[21]

of each agonist was compared to the logarithm of its residence time (Figure 5.9B), a much better correlation was obtained (r^2 = 0.90, p <0.0001), where the highest efficacy ligand UK432,097 had the longest residence time of 250 ± 115 min. In addition, no correlation was observed between functional potency and the logarithm of its residence time (r^2 = 0.077, p = 0.44). The ranking of the relative efficacy, τ, is quite comparable to the intrinsic efficacy, where UK432,097 had the highest τ value of 51 ± 5; LUF5550 had the lowest value of 0.7 ± 0.07 (Table 5.4). Similarly, a positive link between receptor residence time and relative efficacy was observed (r^2 = 0.60, p < 0.01).

Quantification of functional efficacies of $A_{2A}R$ agonists in a cAMP assay

The functional efficacy of all $A_{2A}R$ agonists was tested in a classic cAMP assay as well. The cAMP production was stimulated by adding increasing concentrations of different agonists. The effects were normalized and are

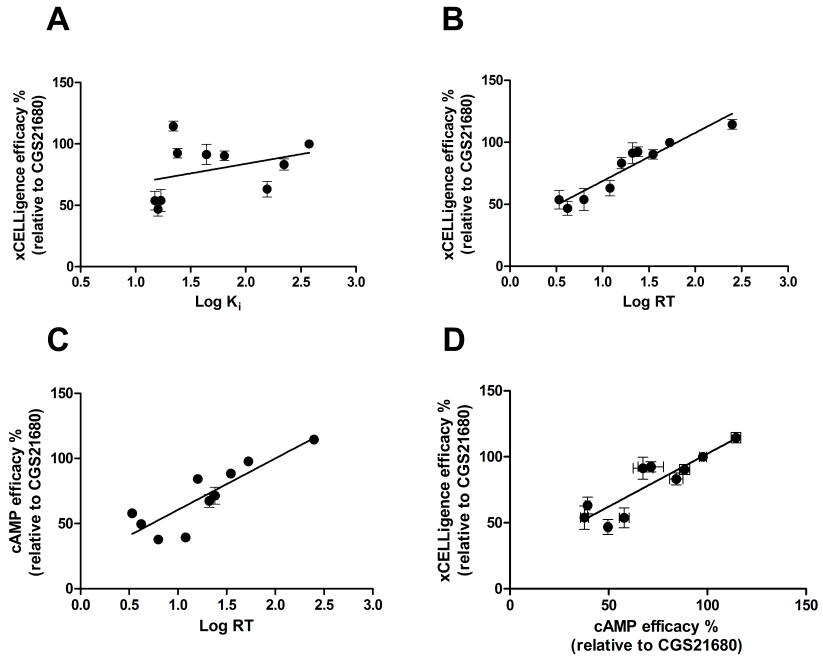

Figure 5.9 | Panel A, correlation of the functional efficacy (E_{max}) derived from label-free whole cell assay against Log K_i (r^2 = 0.13, p = 0.32); Panel B, correlation of the functional efficacy derived from label-free whole cell assay against Log RT (RT, residence time, r^2 = 0.90, $p < 0.0001$). Panel C, correlation of the functional efficacy derived from cAMP assay against Log RT (r^2 = 0.74, $p < 0.001$); Panel D, correlation of the functional efficacy derived from label-free whole cell assay against the functional efficacy derived from cAMP assay (r^2 = 0.79, $p < 0.001$). Data used in these plots are detailed in Table 5.3 and Table 5.4. Data are expressed as mean ± s.e.m. from at least three independent experiments.

shown as a percentage of maximal stimulation of cAMP production by 10 μM CGS21680 (= 100%). Amongst all tested agonists (Figure 5.8C, Table 5.4), UK432,097 had the highest efficacy of 115 ± 2% in this assay. Efficacies of ribose-containing agonists LUF5448, LUF5549, LUF5550 and LUF5631 were 84 ± 3%, 71 ± 6%, 39 ± 1% and 67 ± 5%, while the efficacies of the non-ribose agonists LUF5833, LUF5834 and LUF5835 were 38 ± 2%, 50 ± 1% and 58 ± 2%, respectively. Notably, the ranking of the agonists by their efficacy measured in the cAMP assay is quite comparable to the efficacy-ranking obtained with the impedance-based assay (Figure 5.9D, r^2 = 0.79, p < 0.001). Similarly, a positive link between the functional efficacy and the logarithm of a compound's residence time was observed in this assay as well (Figure 5.9C, r^2 = 0.74, p < 0.001), while no correlation was observed between functional efficacy and the logarithm of its K_i value (r^2 = 0.10, p = 0.40). The ranking of the relative efficacy, τ, in this assay is also quite comparable to that obtained from the whole cell impedance-based assay, where UK432,097 had the highest (τ = 14 ± 5) and LUF5550 had the lowest relative efficacy (τ = 0.5 ± 0.04; Table 5.4). These relative efficacies were again closely correlated to the receptor residence times of the agonists in the present chapter (r^2 = 0.80, p < 0.001).

5.4 Discussion

In this study, the binding kinetics of unlabeled $A_{2A}R$ ligands were determined for the first time using the competition association assay method at the $hA_{2A}R$. This approach has been shown to be highly accurate in determining the binding kinetics at the β-adrenergic receptor[22,23] and more recently at the muscarinic M_3 receptor.[9,24] However, the standard model is laborious and time consuming when the kinetics of multiple compounds need to be determined, since it implies the use of three concentrations of each unlabeled ligand. In this study, the tested agonists were considered competitive with the radioligand as they fully displaced [^{3}H]-ZM241385 from the receptor (Figure 5.3B). Therefore, we modified the three-concentration dependent assay into a one-concentration based method. From Table 5.1, it follows that this simplified method is sufficient in quantifying the binding kinetics, which eventually enables testing in a faster medium-throughput format, yet without loss of accuracy. Since we used an antagonistic radioligand, [^{3}H]-

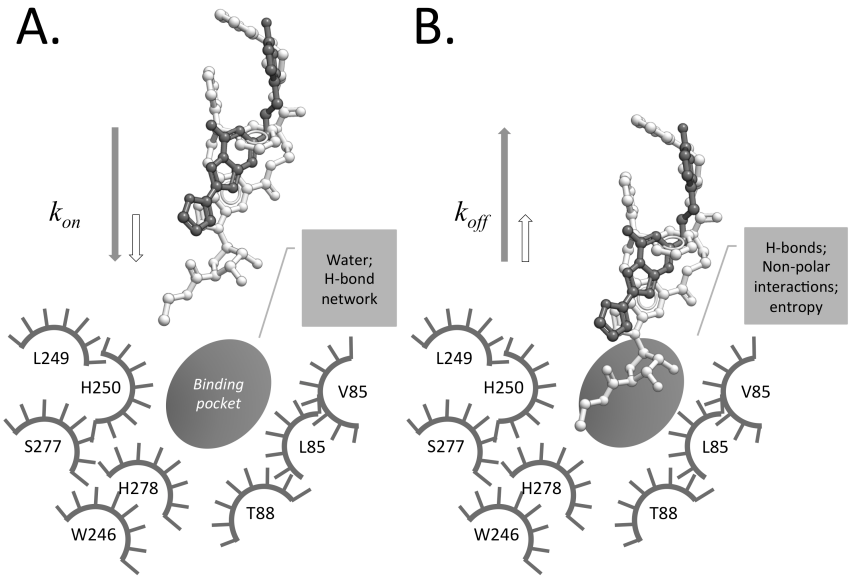

Figure 5.10 | Proposed schematic representation of (Panel A) obstacles at the bottom of the binding pocket and (Panel B) the stabilization effects of the ribose moiety after agonist binding to the receptor. Molecule in black is ZM241385; molecule in white is UK432,097. The length of arrows in black (ZM241385) and white (UK432,097) indicates the speed of ligand association and dissociation. The relative position of these two molecules is coordinated according to the surrounding amino acids based on the crystal structures reported by Jaakola *et al.* (PDB code: 3EML) and Xu *et al.* (PDB code: 3QAK).[29,31] In comparison to ZM241385 (non-ribose compound), UK432,097 (ribose containing compound), binds deeper in the main binding pocket, hence before receptor activation obstacles such as water molecules or structural H-bond networks slow down the association of UK432,097 (Panel A). After ligand binding to the receptor, the ribose part of UK432,097 is stabilized by H-bonds and non-polar interactions and stays in an entropy favorable state after the displacement of explicit water molecules (as present in the ZM241385 crystal structure). This would represent a molecular mechanism accounting for the slower dissociation of ribose containing agonists vs. antagonists (Panel B).

ZM241385, we checked the GTP effect on the equilibrium affinity and the binding kinetics of one representative $A_{2A}R$ agonist, namely NECA. In our system $hA_{2A}R$ was insensitive to GTP (Table 5.2) and only one single binding site was observed (Figure 5.3A). Hence we did not continue to apply GTP in our assays. Subsequent quantification of the binding kinetics of ten $A_{2A}R$ agonists in the simplified model generated comparable 'kinetic K_D' to their K_i values (Table 5.3). This excellent correlation (Figure 5.7B, $r^2 = 0.99$, $p < 0.0001$) proved the accuracy and efficiency of the one-concentration based competition association assay for the determination of a ligand's association and dissociation rates at the $hA_{2A}R$.

To guarantee an accurate kinetic determination, experiments were carried out at 5˚C. Firstly, increasing the experimental temperature resulted in very fast kinetics of the radioligand, which is less practical to quantify the ligand-receptor binding kinetics. Secondly, it is reasonable to speculate that differences in receptor residence times will be more pronounced at 5˚C than at higher temperatures, which would allow an easier identification of compounds with longer residence times in future screening campaigns. It might be argued that such a low temperature cannot be representative for residence times observed *in vivo*. However, it was reported in a guinea pig bronchoconstriction model that UK432,097 (the agonist with the longest residence time in our studies) had a duration of action that lasted over eight hours, whereas the effect of the reference agonist CGS21680 quickly returned to baseline within 60 min.[25,26] Admittedly, the long-lasting effect is likely to be influenced by a number of other factors such as dissolution rate, system pharmacokinetics or tissue residence/rebinding.[27,28] Even so, it is noteworthy that a kinetic difference determined by this protocol (i.e., at 5 ˚C) is still inextricably linked to the *in vivo* efficacy of a drug candidate.

In the present chapter, we observed a broad range of ligand-receptor residence times from 3.4 ± 0.6 min for LUF5835 to 250 ± 115 min for UK432,097. From Table 5.3, it follows that a non-ribose agonist (LUF5833, LUF5834 and LUF5835) associates to the receptor 10-100 fold faster, but remained at the receptor much shorter than a ribose-containing agonist (for structures see Figure 5.1). This observation supports the integral role of a ribose moiety in the binding kinetics upon agonist receptor activation. To activate the $A_{2A}R$, common requirements include the destabilization of H-bond networks at $W246^{6.48}$ and $H278^{7.43}$ (superscripts refer to Ballesteros-Weinstein numbering[46]) and, for example, the displacement of several structural water molecules.[29,30] One can imagine that such 'obstacles' in

the binding cavity will prevent the coordination of the ribose group and, as a result, slow down the agonist association process (Figure 5.10A). The lower on-rates of ribose-containing agonists that were observed compared to those of non-ribose agonists fit this hypothesis. It has been shown that upon receptor activation (Figure 5.10B), the ribose moiety inserts deeply into the binding cavity, as illustrated in the agonist-bound $A_{2A}R$ crystal structures,[31,32] and is stabilized by key residues like S277$^{7.42}$ and H278$^{7.43}$. These residues, together with V84$^{3.32}$, L249$^{6.51}$, are in close contact with the agonist ribose ring, and form essential H-bonds or non-polar interactions with the ribose moiety for agonist binding. Moreover, displacement of the structural water molecules from the hydrophobic pocket favors entropic energy,[33] which further stabilizes the molecule in its interactions and allows it to stay longer. For the co-crystallized UK432,097 in particular it was shown that it has an extensive ligand-receptor interaction network, which includes eleven hydrogen bonds, one aromatic stacking and a number of van der Waals interactions, in the $A_{2A}R$/UK432,097 complex.[31] This further corroborates our finding that UK432,097 has the longest residence-time in the $hA_{2A}R$.

In the present chapter the $A_{2A}R$-mediated activation was determined in two different functional assays, namely, in a novel label-free impedance-based assay (xCELLigence RTCA system), which was compared to a classic cAMP assay. Recently, label-free impedance-based technologies have been shown to have promising applications in assaying functional activity of GPCRs.[34,35] In particular, this assay does not require any labeling or recombinant expression of receptor or reporter proteins, since it is based on detection of cell morphological changes induced by an agonist. Using this impedance-based technology, we were able to discriminate full from partial agonists at the $hA_{2A}R$ (Figure 5.8B and Table 5.4). Their efficacies were similar to those obtained in a traditional cAMP assay (Figure 5.8C and Table 5.4), which indicates that the novel label-free technology is a useful tool to study $A_{2A}R$-mediated activation. Notably, we observed a similar correlation between the residence time of an agonist and its functional efficacy in both assays: rather than the equilibrium affinity, the receptor residence time of an $A_{2A}R$ agonist has a much better correlation to its intrinsic efficacy (Figure 5.9). This correlation was found in other studies as well. For instance, in the case of the α_2-adrenoceptor, the full agonist UK14,304 had a 12-fold longer residence time than the partial agonist clonidine.[36] In another study, Sykes *et al*. tested seven agonists with a broad range of efficacies at the muscarinic M_3 receptor.[9] Similarly, they found that a slowly dissociating M_3 agonist appeared to cause

a higher efficacy in functional assays. Taken together with these observations, our results suggest that receptor residence time and functional efficacies are positively correlated, which may lead us to further understand the molecular basis of agonist functional efficacy at the $hA_{2A}R$.

In the label-free impedance based assay, we observed that the potencies (EC_{50}) of the $A_{2A}R$ agonists were generally higher than the respective binding affinities (compare Table 5.4 to Table 5.3). A similar observation was reported in a study by Dionisotti *et al*. for the functional potency and binding affinity of NECA and CGS21680.[37] Firstly, this discrepancy could be related to the effect of receptor reserve. Occupation of a fraction of the receptor is sufficient to obtain maximal activation in the signal transduction cascade,[37] which is supported by the relative low values of the relative efficacies (Table 5.4). Secondly, we have used an antagonist radioligand ([^{3}H]-ZM241385) to determine agonist affinity, which generally yields lower affinity values than when an agonist radioligand is used.[38-40] It has been shown that the use of an agonistic radioligand, such as [^{3}H]-NECA or [^{3}H]-CGS21680 at the $A_{2A}R$, results in agonist affinities close to their functional potencies.[41,42] In the present chapter, we decided to use an antagonistic radioligand because it recognizes the whole receptor population (G protein-coupled and –uncoupled), which as a result provided a robust condition for kinetic measurements. Moreover, it should be mentioned that the results from the label-free impedance-based assay represent the integration of several signaling pathways, which might explain the difference in agonist potencies obtained in the impedance-based and the cAMP assay. To elaborate this phenomenon, several lines of research indeed indicate that the $A_{2A}R$ can interact with several 'less traditional' scaffold proteins, such as β-arrestin and α-actinin.[43-45] This may further engage cell morphological changes next to effects induced via the classical G_s pathway, and as a result cause an increased, or at least different, potency in a whole cell impedance-based assay. We also explored the relative efficacy, τ, of agonists in the operational model of Black and Leff.[21] Critically, we observed a correlation between the receptor residence time and the relative efficacy in the xCELLigence assay (r^2 = 0.60, p < 0.01) but it was less significant than the correlation found in the cAMP assay (r^2 = 0.80, p < 0.001). This might also be due to the fact that the label-free impedance-based assay combines cell morphological changes induced via several signaling pathways, as stated above.

In summary, we set up and validated a simplified competition association assay at the $hA_{2A}R$, which allowed an accurate and fast measurement of a

ligand's binding kinetics. Agonist efficacy at the $hA_{2A}R$ was determined in a cAMP assay and, for the first time, in a novel label-free impedance-based system. In both functional assays, our data provide evidence that the receptor residence time is correlated to the functional efficacy at the $hA_{2A}R$ rather than the 'traditional' equilibrium affinity of a compound. This finding may lead to a further understanding of the fundamental basis of agonist efficacy at the $hA_{2A}R$.

References:

1. Fredholm BB, IJzerman AP, Jacobson KA, Linden J, Müller CE. International Union of Basic and Clinical Pharmacology. LXXXI. Nomenclature and classification of adenosine receptors--an update. *Pharmacol Rev* 2011;63(1):1-34.
2. Gao ZG, Jacobson KA. Emerging adenosine receptor agonists. *Expert Opin Emerg Drugs* 2007;12(3):479-492.
3. Jacobson KA, Gao ZG. Adenosine receptors as therapeutic targets. *Nat Rev Drug Discov* 2006;5(3):247-264.
4. Copeland RA, Pompliano DL, Meek TD. Drug-target residence time and its implications for lead optimization. *Nat Rev Drug Discov* 2006;5(9):730-739.
5. Swinney DC. Can binding kinetics translate to a clinically differentiated drug? From theory to practice. *Lett Drug Des Discov* 2006;3(8):569-574.
6. Tummino PJ, Copeland RA. Residence time of receptor-ligand complexes and its effect on biological function. *Biochemistry* 2008;47(20):5481-5492.
7. Zhang R, Monsma F. Binding kinetics and mechanism of action: toward the discovery and development of better and best in class drugs. *Expert Opin Drug Discov* 2010;5(11):1023-1029.
8. Copeland RA. *Evaluation of enzyme inhibitors in drug discovery: A guide for medicinal chemists and pharmacologists.* New York: Wiley; 2005. 1-265 p.
9. Sykes DA, Dowling MR, Charlton SJ. Exploring the mechanism of agonist efficacy: a relationship between efficacy and agonist dissociation rate at the muscarinic M_3 receptor. *Mol Pharmacol* 2009;76(3):543-551.
10. Motulsky HJ, Mahan LC. The kinetics of competitive radioligand binding predicted by the law of mass action. *Mol Pharmacol* 1984;25(1):1-9.
11. Van Tilburg EW, Gremmen M, von Frijtag Drabbe Kunzel J, de Groote M, IJzerman AP. 2,8-Disubstituted adenosine derivatives as partial agonists for the adenosine A_{2A} receptor. *Bioorg Med Chem* 2003;11(10):2183-2192.
12. Van Tilburg EW, von Frijtag Drabbe Kunzel J, de Groote M, IJzerman AP. 2,5'-Disubstituted adenosine derivatives: evaluation of selectivity and efficacy for the adenosine A(1), A(2A), and A(3) receptor. *J Med Chem* 2002;45(2):420-429.
13. Beukers MW, Chang LC, von Frijtag Drabbe Kunzel JK, Mulder-Krieger T, Spanjersberg RF, Brussee J, IJzerman AP. New, non-adenosine, high-potency agonists for the human adenosine A_{2B} receptor with an improved selectivity profile compared to the reference agonist

N-ethylcarboxamidoadenosine. *J Med Chem* 2004;47(15):3707-3709.
14. Smith PK, Krohn RI, Hermanson GT, Mallia AK, Gartner FH, Provenzano MD, Fujimoto EK, Goeke NM, Olson BJ, Klenk DC. Measurement of protein using bicinchoninic acid. *Anal Biochem* 1985;150(1):76-85.
15. Xi B, Yu N, Wang X, Xu X, Abassi YA. The application of cell-based label-free technology in drug discovery. *Biotechnol J* 2008;3(4):484-495.
16. Yu N, Atienza JM, Bernard J, Blanc S, Zhu J, Wang X, Xu X, Abassi YA. Real-time monitoring of morphological changes in living cells by electronic cell sensor arrays: an approach to study G protein-coupled receptors. *Anal Chem* 2006;78(1):35-43.
17. Denelavas A, Weibel F, Prummer M, Imbach A, Clerc RG, Apfel CM, Hertel C. Real-time cellular impedance measurements detect $Ca^{(2+)}$ channel-dependent oscillations of morphology in human H295R adrenoma cells. *Biochim Biophys Acta* 2011;1813(5):754-762.
18. Flynn AN, Tillu DV, Asiedu MN, Hoffman J, Vagner J, Price TJ, Boitano S. The protease-activated receptor-2-specific agonists 2-aminothiazol-4-yl-LIGRL-NH2 and 6-aminonicotinyl-LIGRL-NH_2 stimulate multiple signaling pathways to induce physiological responses *in vitro* and *in vivo*. *J Biol Chem* 2011;286(21):19076-19088.
19. Scandroglio P, Brusa R, Lozza G, Mancini I, Petro R, Reggiani A, Beltramo M. Evaluation of cannabinoid receptor 2 and metabotropic glutamate receptor 1 functional responses using a cell impedance-based technology. *J Biomol Screen* 2010;15(10):1238-1247.
20. Cheng Y, Prusoff WH. Relationship between the inhibition constant (K_1) and the concentration of inhibitor which causes 50 per cent inhibition (I_{50}) of an enzymatic reaction. *Biochem Pharmacol* 1973;22(23):3099-3108.
21. Black JW, Leff P. Operational models of pharmacological agonism. *Proc R Soc Lond B Biol Sci* 1983;220(1219):141-162.
22. Affolter H, Hertel C, Jaeggi K, Portenier M, Staehelin M. (-)-S-[^{3}H]CGP-12177 and its use to determine the rate constants of unlabeled beta-adrenergic antagonists. *Proc Natl Acad Sci U S A* 1985;82(3):925-929.
23. Contreras ML, Wolfe BB, Molinoff PB. Kinetic analysis of the interactions of agonists and antagonists with beta adrenergic receptors. *J Pharmacol Exp Ther* 1986;239(1):136-143.
24. Dowling MR, Charlton SJ. Quantifying the association and dissociation rates of unlabeled antagonists at the muscarinic M_3 receptor. *Br J Pharmacol* 2006;148(7):927-937.
25. Mantell SJ, Stephenson PT, Monaghan SM, Maw GN, Trevethick MA, Yeadon M, Keir RF, Walker DK, Jones RM, Selby MD, Batchelor DV, Rozze S, Chavaroche H, Hobson TJ, Dodd PG, Lemaitre A, Wright KN, Stuart EF. Inhaled adenosine A(2A) receptor agonists for the treatment of chronic obstructive pulmonary disease. *Bioorg Med Chem Lett* 2008;18(4):1284-1287.
26. Mantell SJ, Stephenson PT, Monaghan SM, Maw GN, Trevethick MA, Yeadon M, Walker DK, Selby MD, Batchelor DV, Rozze S, Chavaroche H, Lemaitre A, Wright KN, Whitlock L, Stuart EF, Wright PA, Macintyre F. SAR of a series of inhaled A(2A) agonists and comparison of inhaled pharmacokinetics in a preclinical model with clinical pharmacokinetic data. *Bioorg Med Chem Lett* 2009;19(15):4471-4475.
27. Vauquelin G. Rebinding: or why drugs may act longer in vivo than expected from their in vitro target residence time. *Expert Opin Drug Discov* 2010;5(10):927-941.
28. Vauquelin G, Van Liefde I. Slow antagonist dissociation and long-lasting *in vivo* receptor protection. *Trends Pharmacol Sci* 2006;27(7):356-359.
29. Jaakola VP, Griffith MT, Hanson MA, Cherezov V, Chien EY, Lane JR, IJzerman AP, Stevens RC. The 2.6 angstrom crystal structure of a human A_{2A} adenosine receptor bound to an antagonist.

Science 2008;322(5905):1211-1217.
30. Kim SK, Gao ZG, Van Rompaey P, Gross AS, Chen A, Van Calenbergh S, Jacobson KA. Modeling the adenosine receptors: comparison of the binding domains of A_{2A} agonists and antagonists. *J Med Chem* 2003;46(23):4847-4859.
31. Xu F, Wu H, Katritch V, Han GW, Jacobson KA, Gao ZG, Cherezov V, Stevens RC. Structure of an agonist-bound human A_{2A} adenosine receptor. *Science* 2011;332(6027):322-327.
32. Lebon G, Warne T, Edwards PC, Bennett K, Langmead CJ, Leslie AG, Tate CG. Agonist-bound adenosine A_{2A} receptor structures reveal common features of GPCR activation. *Nature* 2011;474(7352):521-525.
33. Borea PA, Dalpiaz A, Varani K, Gessi S, Gilli G. Binding thermodynamics at A_1 and A_{2A} adenosine receptors. *Life Sci* 1996;59(17):1373-1388.
34. McGuinness R. Impedance-based cellular assay technologies: recent advances, future promise. *Curr Opin Pharmacol* 2007;7(5):535-540.
35. Peters MF, Scott CW. Evaluating cellular impedance assays for detection of GPCR pleiotropic signaling and functional selectivity. *J Biomol Screen* 2009;14(3):246-255.
36. Hoeren M, Brawek B, Mantovani M, Löffler M, Steffens M, Velthoven V, Feuerstein TJ. Partial agonism at the human α_{2A}-autoreceptor: role of binding duration. *Naunyn-Schmiedeberg's Arch Pharmacol* 2008;378(1):17-26.
37. Dionisotti S, Ongini E, Zocchi C, Kull B, Arslan G, Fredholm BB. Characterization of human A_{2A} adenosine receptors with the antagonist radioligand [^{3}H]-SCH 58261. *Br J Pharmacol* 1997;121(3):353-360.
38. Bruns RF, Fergus JH, Badger EW, Bristol JA, Santay LA, Hays SJ. PD 115,199: an antagonist ligand for adenosine A_2 receptors. *Naunyn-Schmiedeberg's Arch Pharmacol* 1987;335(1):64-69.
39. Nonaka H, Mori A, Ichimura M, Shindou T, Yanagawa K, Shimada J, Kase H. Binding of [^{3}H] KF17837S, a selective adenosine A_2 receptor antagonist, to rat brain membranes. *Mol pharmacol* 1994;46(5):817-822.
40. Zocchi C, Ongini E, Ferrara S, Baraldi PG, Dionisotti S. Binding of the radioligand [^{3}H]-SCH 58261, a new non-xanthine A_{2A} adenosine receptor antagonist, to rat striatal membranes. *Brit J Pharmacol* 1996;117(7):1381-1386.
41. Jarvis MF, Schulz R, Hutchison AJ, Do UH, Sills MA, Williams M. [^{3}H]CGS21680, a selective A_2 adenosine receptor agonist directly labels A_2 receptors in rat brain. *J Pharmacol Exp Ther* 1989;251(3):888-893.
42. Müller CE, Maurinsh J, Sauer R. Binding of [^{3}H]MSX-2 (3-(3-hydroxypropyl)-7-methyl-8-(m-methoxystyryl)-1-propargylxanthine) to rat striatal membranes--a new, selective antagonist radioligand for A_{2A} adenosine receptors. *Eur J Pharm Sci* 2000;10(4):259-265.
43. Verzijl D, IJzerman AP. Functional selectivity of adenosine receptor ligands. *Purinergic Signal* 2011;7(2):171-192.
44. Burgueno J, Blake DJ, Benson MA, Tinsley CL, Esapa CT, Canela EI, Penela P, Mallol J, Mayor F, Jr., Lluis C, Franco R, Ciruela F. The adenosine A_{2A} receptor interacts with the actin-binding protein alpha-actinin. *J Biol Chem* 2003;278(39):37545-37552.
45. Keuerleber S, Gsandtner I, Freissmuth M. From cradle to twilight: the carboxyl terminus directs the fate of the A(2A)-adenosine receptor. *Biochim Biophys Acta* 2011;1808(5):1350-1357.
46. Ballesteros JA, Weinstein H. Integrated methods for the construction of three dimensional models and computational probing of structure–function relations in G-protein coupled receptors. *Methods Neurosci* 1995;25:366–428.